Supporting information for

Surface and Lattice Engineered Ruthenium Superstructures towards High-Performance Bifunctional Hydrogen Catalysis

Leigang Li,[a] Shangheng Liu,[a] Changhong Zhan,[a] Yan Wen,[a] Zhefei Sun,[b] Jiajia Han,[*b] Ting-Shan Chan,[c] Qiaobao Zhang,[*b] Zhiwei Hu,[d] Xiaoqing Huang[*a]

E-mail: jiajiahan@xmu.edu.cn; zhangqiaobao@xmu.edu.cn; hxq006@xmu.edu.cn

Experimental Procedures

1.1 Synthesis of Mo-Ru NSAs

For the typical synthesis of Mo-Ru NSAs, 8.0 mg ruthenium carbonyl ($Ru_3(CO)_{12}$, > 98%, from dramas-beta), 2.5 mg molybdenum carbonyl ($Mo(CO)_6$, 98%, from Sigma Aldrich), 30 mg salicylic acid ($C_7H_6O_3$, ≥ 99.5%, Sinopharm Chemical Reagent Co.), and 5.0 mL oleylamine (OAm, $C_{18}H_{37}N$, from J&K Scientific Ltd.) were put in a glass vial and homogeneously mixed by ultrasonication. The glass vial was then transferred into an oil bath and heated at 230 ^oC for 3 h. After cooling down to room temperature, the product was collected by high-speed centrifugation and washed for three times with a mixture of cyclohexane/ethanol.

1.2 Characterization

The morphology of the synthesized sample was firstly characterized by a low-magnification transmission electron microscope (TEM, Hitachi HT7700, 120 kV). An FEI Tecnai F20 TEM (200 kV) was employed to get the HAADF STEM images, high-magnification TEM images, and EDS line scan/mapping. The TEM sample for characterization was prepared by dropping cyclohexane dispersion of the synthesized product onto a carbon-coated Cu grid and dried at ambient conditions. An energy dispersive X-ray spectrometer coupled within a Zeiss scanning electron microscope was used to acquire the chemical composition. The XRD pattern was obtained by a X'Pert-Pro MPD diffractometer with a Cu K_α X-ray source (λ = 1.540598 Å). An SSI S-Probe XPS spectrometer was employed to acquire the surface chemical information. The XAS spectra were acquired at the BL01C1 beamline of the National Synchrotron Radiation Research Center (NSRRC, Hsinchu, Taiwan). The data were processed according to standard procedures using the software of Demeter program package (Version 0.9.24).[1]

1.3 Electrochemical measurement

The HER performance of the catalysts was evaluated by a three-electrode system on an electrochemical station (CHI660, Chenhua, Shanghai). For the typical preparation of catalyst ink, a certain amount of catalyst was dissolved in a mixture of isopropanol and Nafion (volume ratio, 50:1) to get a catalyst concentration of 1 μg/μL. The mixture was homogeneously mixed by ultrasonication for 30 min to get the catalyst ink. The catalyst ink (10 μL) was then dropped onto a glassy carbon (GC) electrode (0.196 cm^2) and dried naturally as the working electrode. A graphite rod and a saturated calomel electrode (SCE) was used as the counter electrode and reference electrode, respectively. The electrochemical test was performed in 1 M KOH. For linear sweep voltammetry (LSV) polarization scan, a scan rate of 5 mV/s is used. A rotating disk electrode (RDE, Pine, diameter: 5 mm) was used

to measure the HOR performance with a graphite rod as the counter electrode and a SCE as the reference electrode, respectively. The measurement was performed in H_2-saturated 0.1 M KOH electrolyte at a scan rate of 5 mV/s. Catalyst ink with a Ru concentration of 0.5 μg/μL was prepared and 2 μL catalyst ink was dropped onto the RDE which was dried naturally under ambient atmosphere. All the potentials in SCE were transformed to reversible hydrogen electrode (RHE) potentials. During the LSV measurement, 95% iR compensation was applied.

For HOR, the kinetic current density (j_k) was analyzed by the Koutecky-Levich equation:

$$\frac{1}{j} = \frac{1}{j_k} + \frac{1}{j_d}$$

where j is the measured current density and j_d is the diffusion-limited current density. j_k and j_d can be fitted using the Butler-Volmer equation and Levich equation, respectively.

$$j_k = j_0(e^{\frac{\alpha_a F\eta}{RT}} - e^{-\frac{\alpha_c F\eta}{RT}})$$

$$j_d = 0.62\mathrm{nF}D^{3/2}\nu^{-1/6}\mathrm{C}_0\omega^{1/2} = \mathrm{BC}_0\omega^{1/2}$$

where α_a and α_c are anodic and cathodic electron transfer coefficient, respectively ($\alpha_a + \alpha_c = 1$), F the Faraday constant, η the overpotential, R the universal gas constant, T the Kelvin temperature, n the electron number, D the diffusion coefficient, ν the viscosity coefficient, C_0 the solubility, ω the rotating speed, and B the Levich constant.

1.4 DFT

Spin-polarized DFT calculations were performed by using Vienna Ab initio Simulation Package (VASP).[2] The Perdew-Burke-Erzenhof (PBE) functional in the generalized gradient approximation (GGA) was applied to describe the exchange-correlation energy.[3] The wave functions were employed in a plane wave basis set with an energy cutoff of 600 eV. The convergence criteria for energy and force were set to be 10^{-5} eV and 0.02 eV/Å, respectively. The zero damping DFT–D3 method of Grimme[4] was adopted in describing van der Waals interactions. The 4×4×1 supercell of Ru(101) and Ru(002) facet with six layers was taken as the substrate model with a Gamma centered 3 × 3 × 1 k–point mesh. To reproduce the bulk properties, two bottom layers were fixed. The Brillouin zone was sampled by Gamma centered 3×3×1 Monkhorst-Pack grid for structural optimizations. All the slab models were separated by a vacuum of 15 Å thickness to ensure decoupling between neighboring slabs.

The adsorption free energy (ΔG) as a result of electrochemical adsorption reactions is calculated using the following expression:

$$\Delta G = \Delta E + \Delta E_{\mathrm{ZPE}} - T\Delta S$$

where ΔE is the change in total energy obtained from DFT, ΔE_{ZPE} and S are the changes in zero-point energy and entropy at standard conditions with T = 298.15 K.

The adsorption energy ΔE for a given site is defined as

$$\Delta E = E_{\mathrm{surf+ads}} - E_{\mathrm{surf}} - E_{\mathrm{ads}}$$

where E_{surf} is the surface energy, E_{ads} is the energy of adsorbate, and $E_{\mathrm{surf+ads}}$ is the total system energy.

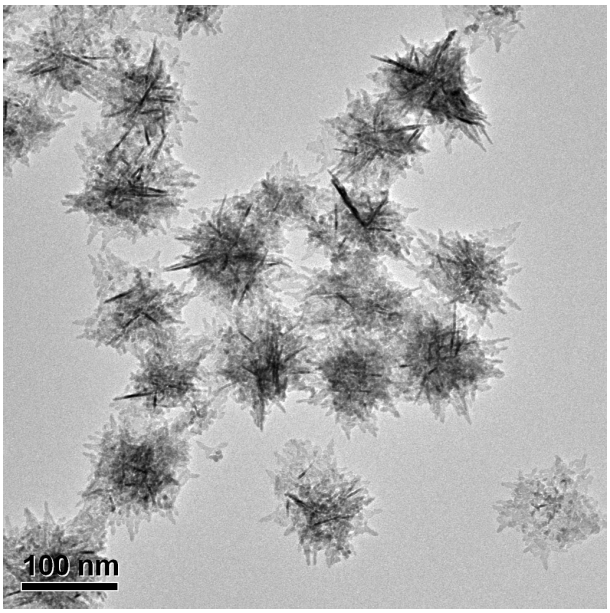

Figure S1. TEM image of Mo-Ru NSAs.

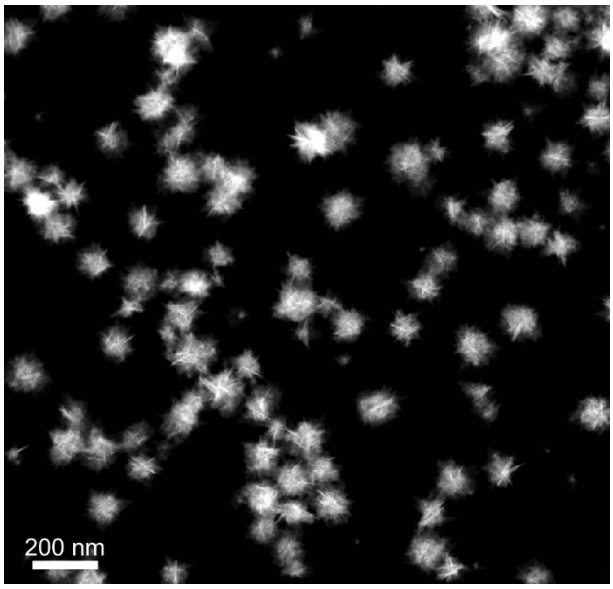

Figure S2. STEM image of Mo-Ru NSAs.

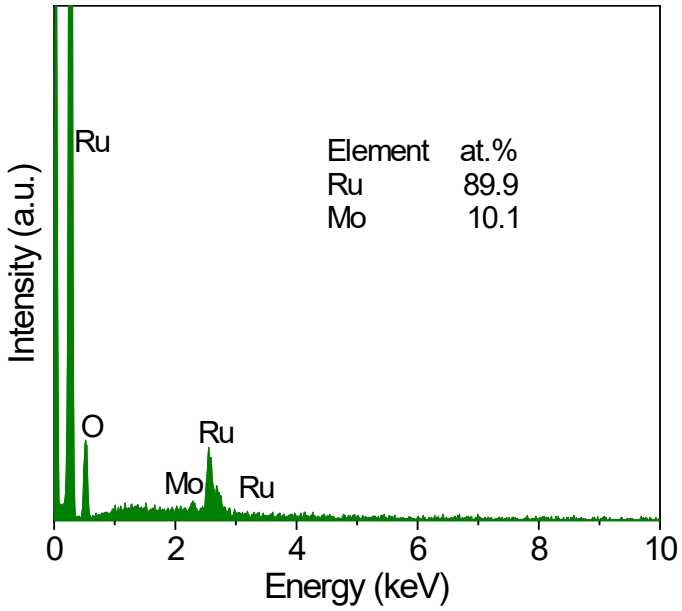

Figure S3. EDS spectrum showing the chemical composition of Mo-Ru NSAs.

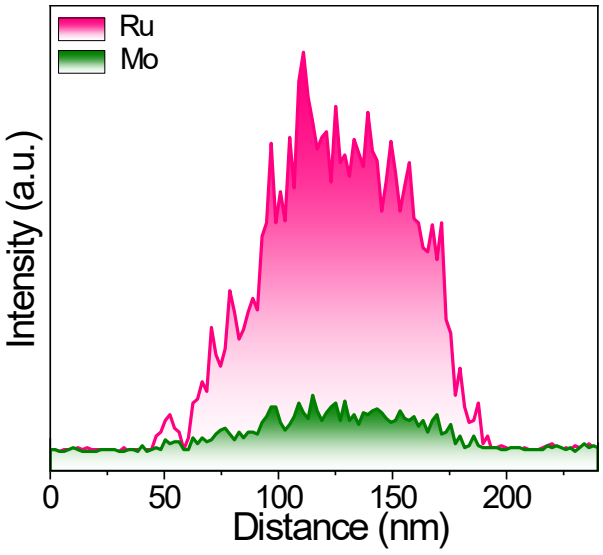

Figure S4. EDS line scan of Mo-Ru NSAs.

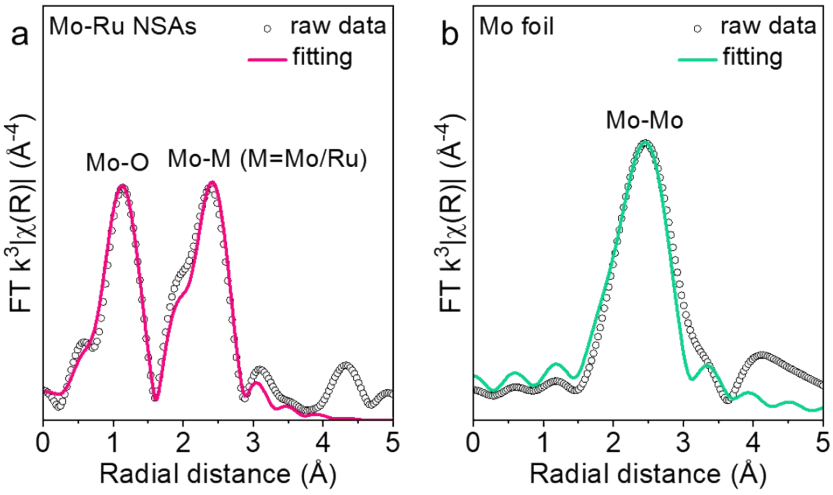

Figure S5. k^3-weighted Fourier transformation and fitting of EXAFS spectra of (a) Mo-Ru NSAs and (b) Mo foil in R space.

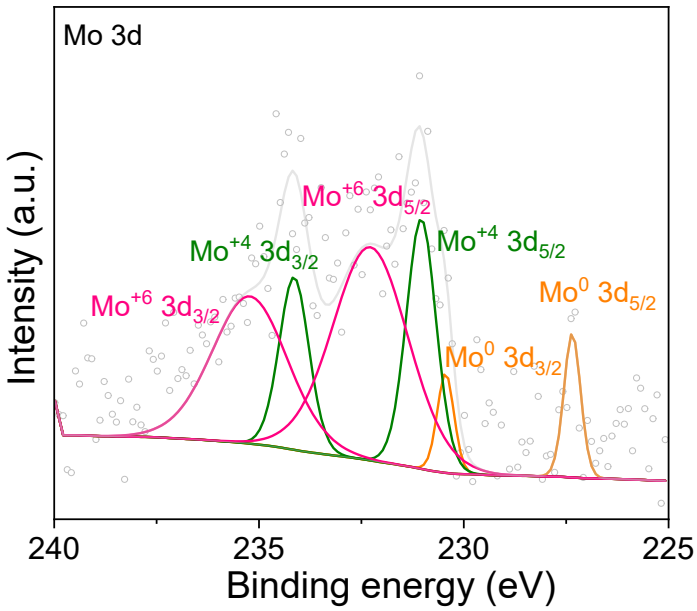

Figure S6. Mo 3d XPS spectrum of Mo-Ru NSAs.

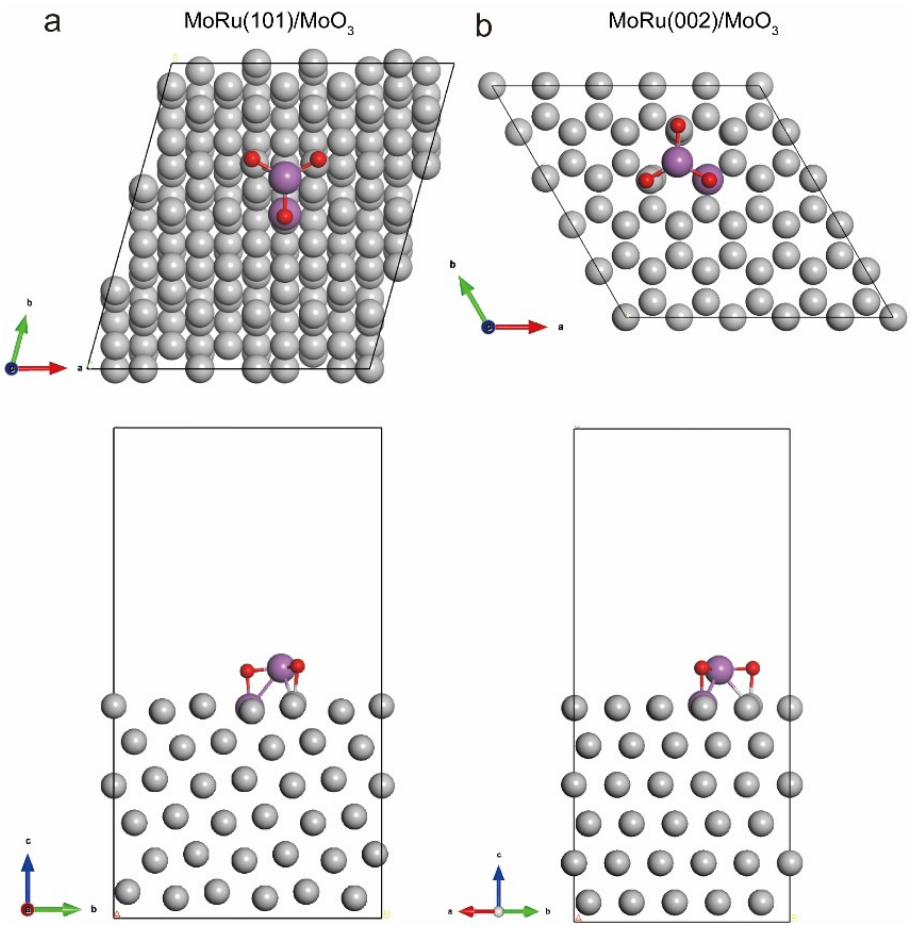

Figure S7. Atomic structures of (a) MoRu(101)/MoO_3 and (b) MoRu(002)/MoO_3.

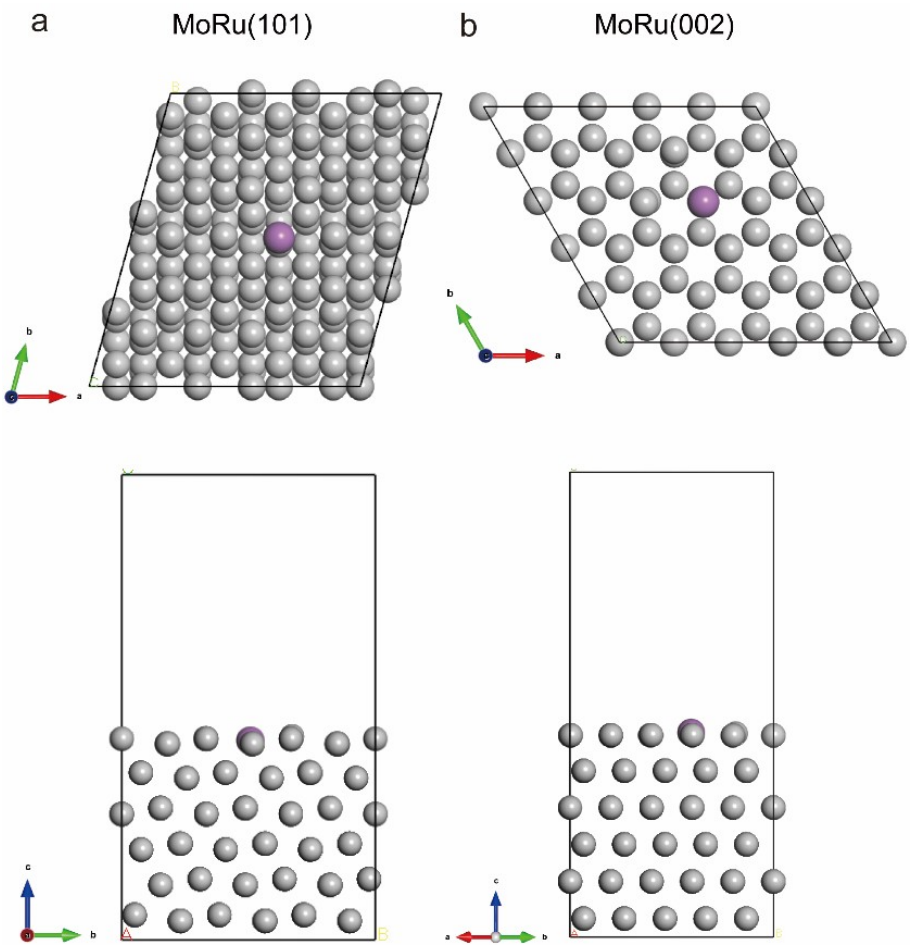

Figure S8. Atomic structures of (a) MoRu(101) and (b) MoRu(002).

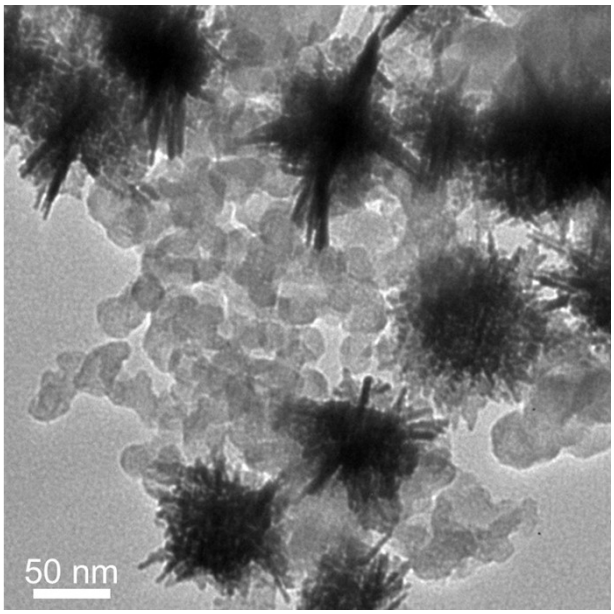

Figure S9. TEM image of Mo-Ru NSAs loaded on carbon powder.

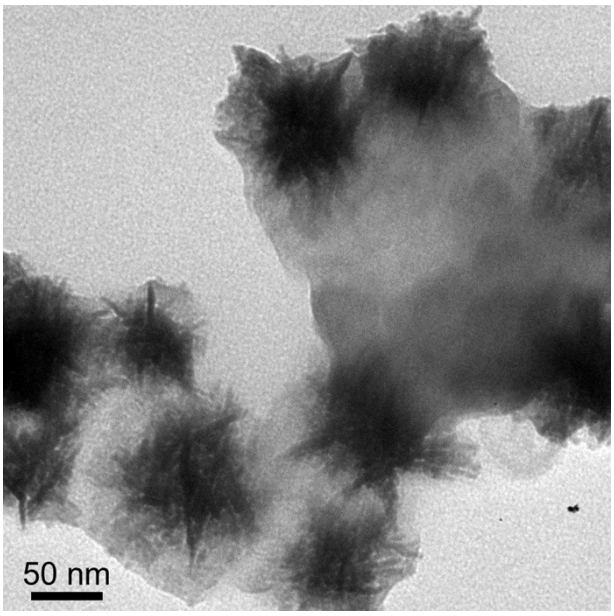

Figure S10. TEM image of Mo-Ru NSAs annealed at 250 °C for 0.5 h in air.

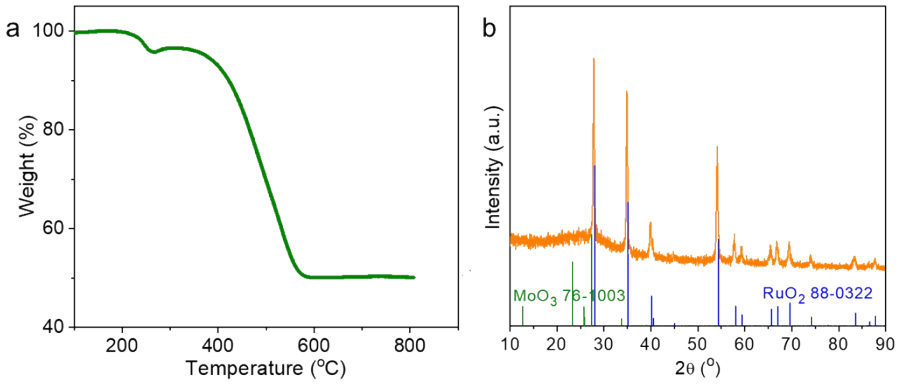

Figure S11. (a) TG plot of Mo-Ru NSAs. (b) XRD pattern of Mo-Ru NSAs annealed at 800 ^{o}C in air.

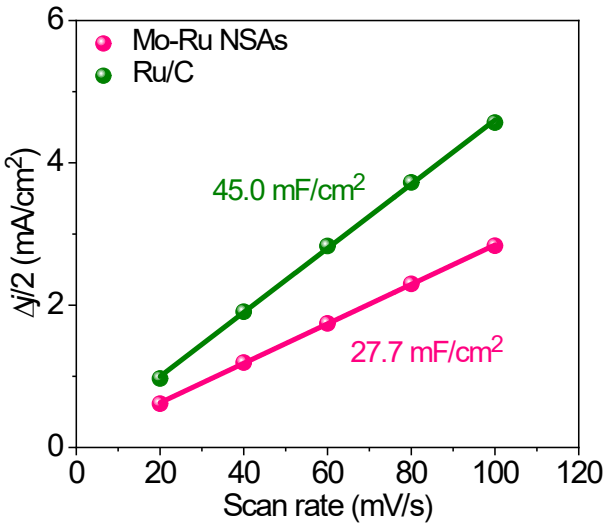

Figure S12. Electrochemical double-layer capacitance (C_{dl}) of Mo-Ru NSAs and commercial Ru/C.

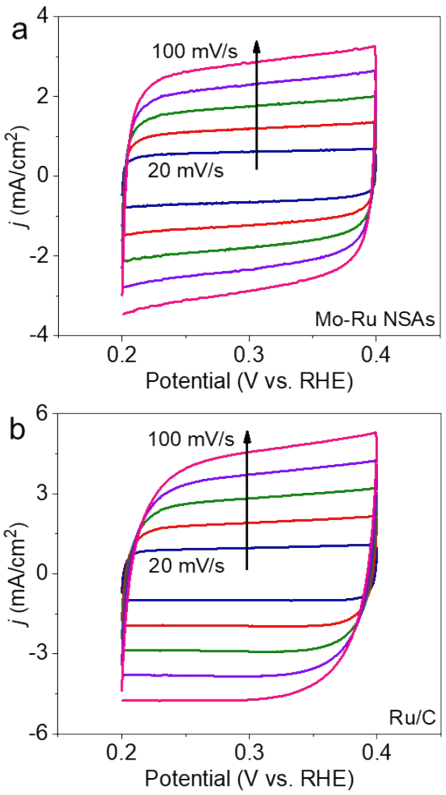

Figure S13. CV scans of (a) Mo-Ru NSAs and (b) commerical Ru/C.

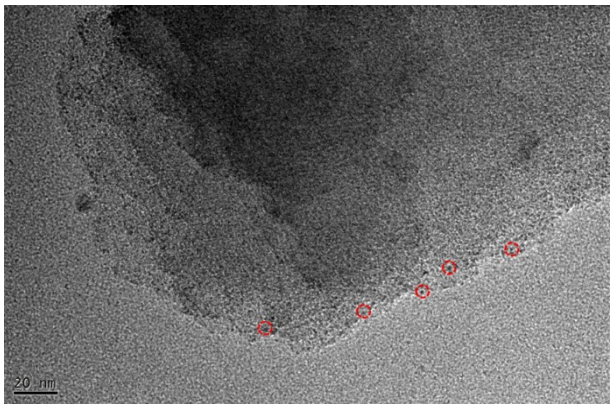

Figure S14. TEM image of commercial Ru/C.

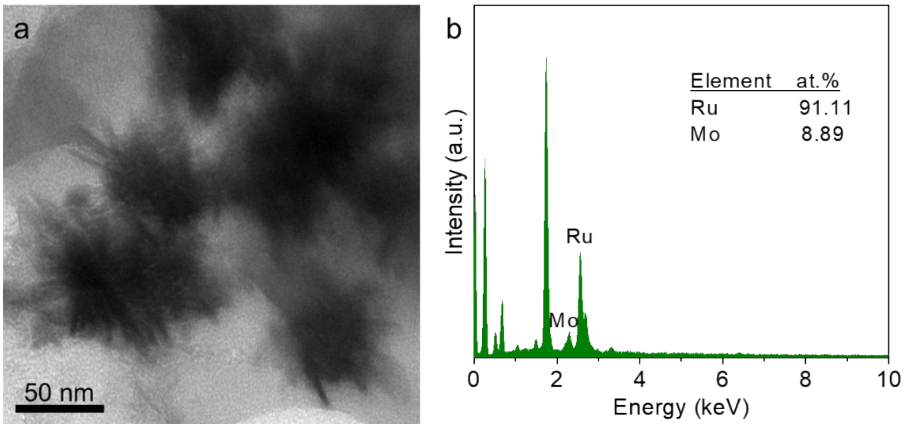

Figure S15. (a) TEM image and (b) EDS spectrum of Mo-Ru NSAs after HER stability test.

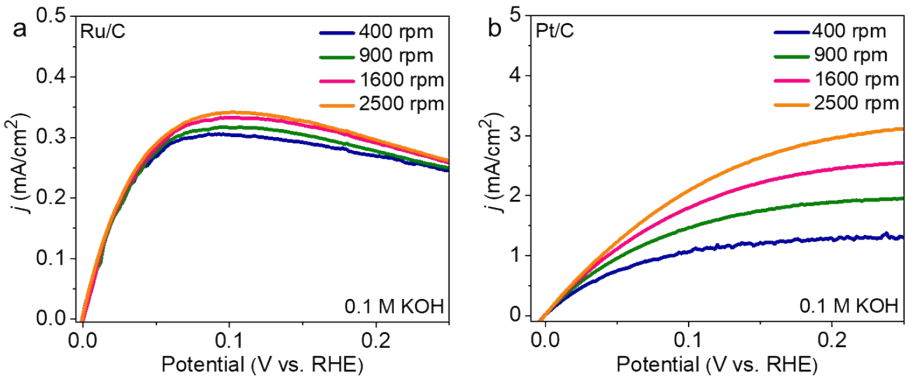

Figure S16. HOR polarization curves of commercial (a) Ru/C and (b) Pt/C in H_2-saturated 0.1 M KOH.

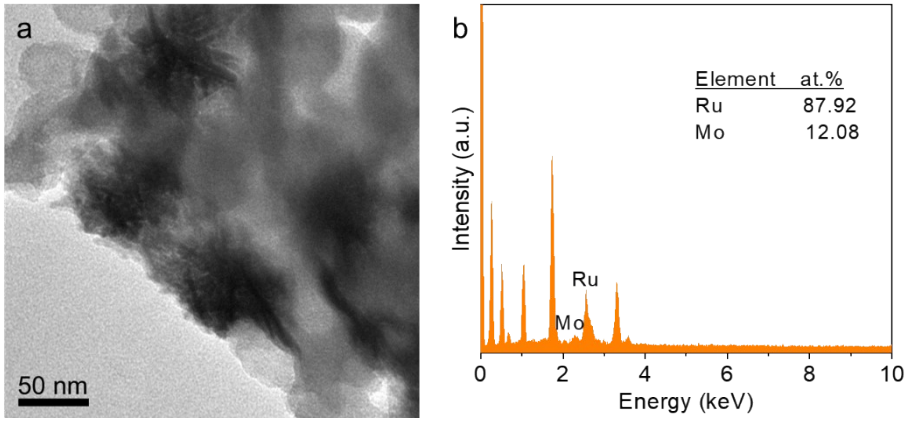

Figure S17. (a) TEM image and (b) EDS spectrum of Mo-Ru NSAs after HOR stability test.

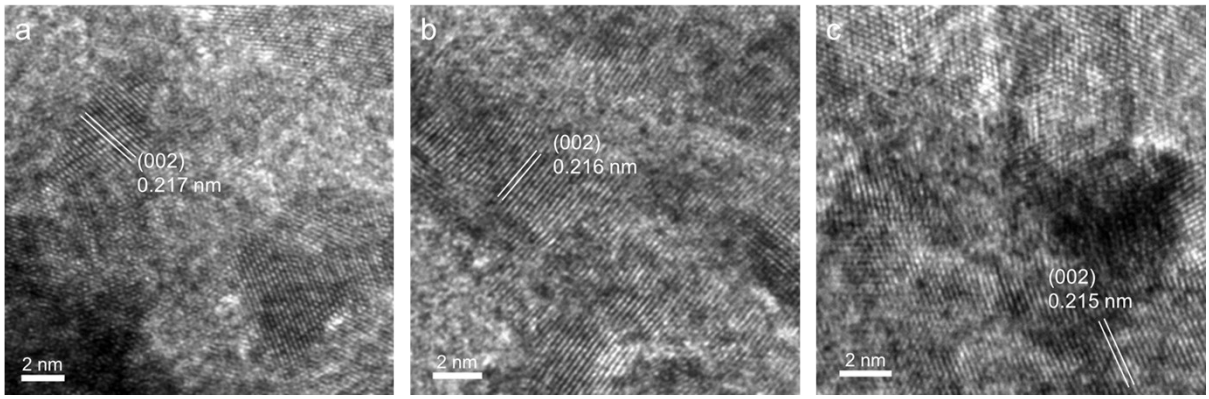

Figure S18. TEM images of Mo-Ru NSAs (a) before stability test, (b) after HER stability test, and (c) after HOR stability test.

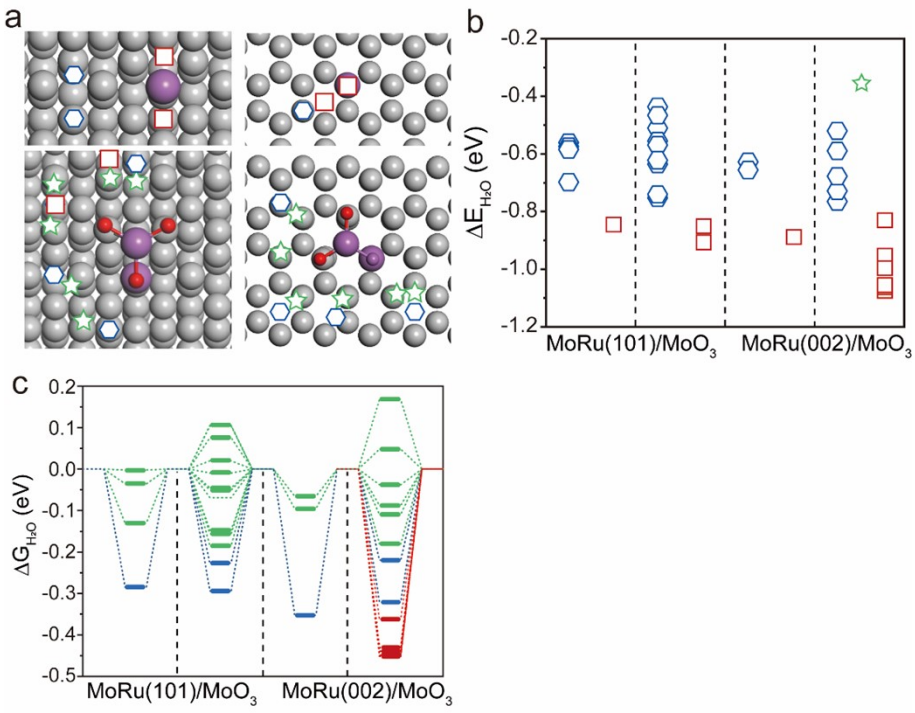

Figure S19. (a) Diagram of corresponding adsorption sites of OH^*, where green five-pointed stars, blue hexagons and red squares represent weakly, moderately and strongly adsorbed sites, respectively. (b) Adsorption energy ΔE of H_2O^* at different adsorption sites of different surfaces. (c) Gibbs free energy diagrams of absorbed H_2O^* on different surfaces.

Table S1. Structural parameters of the samples obtained from EXAFS fitting for Ru K-edge.

sample	path	N	R (Å)	ΔE_0 (eV)	σ^2 ($\times 10^{-3}$Å^2)	R-factor
Mo-Ru NSAs	Ru-Ru	5.4±0.9	2.68±0.01	-5.78±1.51	5.03±0.94	0.015
	Ru-O	2.7±1.5	1.94±0.05	-9.68±9.80	7.78±6.28	
Ru foil	Ru-Ru	12	2.67±0.03	9.02±0.66	3.60±0.40	0.009

N, coordination number; R, distance between absorber and backscatter atoms; ΔE_0, inner potential correction to account for the difference in the inner potential between the sample and the reference compound. σ^2, Debye-Waller factor.

Table S2. Structural parameters of the samples obtained from EXAFS fitting for Mo K-edge.

sample	path	N	R (Å)	ΔE_0 (eV)	σ^2 ($\times 10^{-3}$Å^2)	R-factor
Mo-Ru NSAs	Mo-Mo1	2.9±1.2	2.73±0.04	-5.81±3.14	8.14±3.47	0.014
	Mo-O	3.2±1.6	1.72±0.04	-18.0±8.10	8.70±5.47	
Mo foil	Mo-Mo1	8	2.72±0.01	-6.21±1.28	2.66±0.95	0.001
	Mo-Mo2	6	3.15±0.02	-3.96±2.66	2.25±1.42	

N, coordination number; R, distance between absorber and backscatter atoms; ΔE_0, inner potential correction to account for the difference in the inner potential between the sample and the reference compound. σ^2, Debye-Waller factor.

Table S3. Comparison of HER performance of various catalysts in alkaline electrolytes.

Catalyst	Electrolyte	Overpotential (mV) at 10 mA/cm^2	Ref.
Mo-Ru NSAs	**1 M KOH**	**16**	**This work**
Ru/N-doped C	1 M KOH	32	*Energy Environ. Sci.* **2018**, *11*, 800
Ru@C_2N	1 M KOH	17	*Nat. Nanotechnol.* **2017**, 12, 441-446
Pt_3Ni_2-NWs-S	1 M KOH	42	*Nat. Commun.* **2017**, *8*, 14580
Pt NWs	1 M KOH	50	*Adv. Funct. Mater.* **2018,** 28**, 1803722**
RuP_2@NPC	1 M KOH	52	*Angew. Chem. Int. Ed.* **2017**, *56*, 11559
Ru/MoO_2	1 M KOH	29	*J. Mater. Chem. A* **2017**, *5*, 5475
NiO/Ru@porous Ni	1 M KOH	39	*J. Mater. Chem. A* **2019**, *7*, 2344
Ru_3Ni_3	1 M KOH	39	*iScience* **2019**, *11*, 492
a-$RuTe_2$ PNRs	1 M KOH	36	*Nat. Commun.* **2019**, *10*, 5692
RuP/C	1 M KOH	18	*Adv. Mater.* **2018**, 30, 1800047
RuCu NSs	1 M KOH	20	*Angew. Chem. Int. Ed.* **2019**, *58*, 13983
RuMn NSBs	1 M KOH	20	*Adv. Mater.* **2021**, 2105308
Sr_2RuO_4	1 M KOH	61	*Nat. Commun.* **2019**, *10*, 149
Ir NWs	1 M KOH	38	*Adv. Funct. Mater.* **2018,** *28*, 1803722
$Cu_{2-x}S$/Ru	1 M KOH	82	*Small* **2017**, *13*, 1700052
Pt-Ni ASs	1 M KOH	27.7	*Adv. Mater.* **2018**, 1801741
Ru-S-2/C	1 M KOH	40	*Catal. Sci. Technol.* **2021**, *11*, 3865-3872
Ru-NiCo-LDH	1 M KOH	28	*Electrochem. Commun.*

			2019, *101*, 23-27
Pd_3Ru/C	1 M KOH	42	*ACS Catal.* **2019**, *9*, 9614-9621

Table S4. Comparison of HOR performance of various catalysts in alkaline electrolytes.

Catalyst	Electrolyte	Mass activity (A/mg)	Ref.
Mo-Ru NSAs	**0.1 M KOH**	**2.45**	**This work**
$Ir_3Pd_1Ru_6$	0.1 M KOH	0.34	*J. Am. Chem. Soc.* **2017**, *139*, 6807-6810
Ru nanoassembly	0.1 M KOH	0.0376	*Appl. Catal. B-Environ.* **2019**, *258*, 117952
Mo-Ru-2/C	0.1 M KOH	1.86	*ACS Sustainable Chem. Eng.* **2022**, *10*, 1616-1623
fcc Ru	0.1 M KOH	0.1204	*J. Energy Chem.* **2021**, *61*, 15-22
Ir_9Ru_1/C	0.1 M KOH	0.74	*J. Am. Chem. Soc.* **2017**, *139*, 6807-6810
P-Rh/C	0.1 M KOH	0.683	*J. Mater. Chem. A* **2020**, *8*, 11923-11927
BCC PdCu	0.1 M KOH	1.727	*J. Am. Chem. Soc.* **2018**, *140*, 16580-16588
IrNi@PdIr/C	0.1 M KOH	0.854	*Nanoscale* **2018**, *10*, 4872-4881
IO-Ru-TiO_2/C	0.1 M KOH	0.907	*J. Mater. Chem. A* **2020**, *8*, 10168-10174
PtNb/NbO_x-C	0.1 M KOH	0.36	*ACS Catal.* **2017**, *7*, 4936-4946
$Ru_{0.95}Fe_{0.05}$ NPs	0.1 M KOH	0.16	*ACS Catal.* **2020**, *10*, 4608-4616
$IrMo_{0.59}$ NPs	0.1 M KOH	0.5	*ACS Catal.* **2020**, *10*, 7322-7327
Ru-Ir(1/1)	0.1 M NaOH	0.22	*ACS Appl. Mater. Interfaces* **2020**, *12*, 22771-22777
P-Ru/C	0.1 M KOH	0.43	*ACS Catal.* **2020**, *10*, 11751-11757
PtRu/Mo_2C-TaC	0.1 M KOH	0.403	*ACS Catal.* **2021**, *11*, 932-947
PtRu/Mo_2C	0.1 M KOH	0.239	*ACS Catal.* **2021**, *11*, 932-947

hcp Ru	0.1 M KOH	0.08721	*J. Energy Chem.* **2021**, *61*, 15-22
$Ru@Pt_{1.4MLE}$	0.1 M NaOH	1.309	*J. Electrochem. Soc.* **2018**, *165*, H229-H239
Ru/C	0.1 M NaOH	0.022	*ACS Appl. Mater. Interfaces* **2020**, *12*, 22771-22777

References

1. B. Ravel and M. Newville, *J. Synchrotron Radiat.* 2005, **12**, 537-541.
2. G. Kresse and J. Furthmüller, *Phys. Rev. B* 1996, **54**, 11169-11186.
3. J. P. Perdew, K. Burke and M. Ernzerhof, *Phys. Rev. Lett.* 1996, **77**, 3865-3868.
4. S. Grimme, *J. Comput. Chem.* 2006, **27**, 1787-1799.